Journal of Materials Chemistry A

The Stabilization of Supported Au Nanoparticles in a Highly Sintering Environment using High Surface Free Energy Pt and Ru Cores

Journal:	*Journal of Materials Chemistry A*
Manuscript ID	TA-ART-04-2021-002956.R1
Article Type:	Paper
Date Submitted by the Author:	31-May-2021
Complete List of Authors:	O-Connell, Kerry; University of South Carolina , Department of Chemical Engineering Monnier, John; University of South Carolina System, Department of Chemical Engineering Regalbuto, John; University of South Carolina , Department of Chemical Engineering

The Stabilization of Supported Au Nanoparticles in a Highly Sintering Environment using High Surface Free Energy Pt and Ru Cores

Kerry C. O'Connell, and John R. Monnier, and J.R. Regalbuto*

Department of Chemical Engineering, University of South Carolina, 301 Main St., Columbia, SC 29208

(*) regalbuj@cec.sc.edu

Abstract

To stabilize carbon supported gold nanoparticles which sinter rapidly in a highly corrosive chemical environment containing gaseous HCl at elevated temperature (180°C), bimetallic Ru@Au and Pt@Au core-shell supported nanoparticles were prepared by anchoring shells of Au onto higher surface free energy cores of Pt and Ru. Highly dispersed (sub-2 nm) Pt and Ru particles prepared by electrostatic adsorption of the respective precursors onto the carbon support were themselves stable in the corrosive medium. As confirmed by XRD, chemisorption, and HRTEM analyses of the fresh and treated nanoparticles, Au shells deposited onto the Pt and Ru metal cores were completely stabilized against sintering and in fact appeared to spread on the high surface free energy metal core surfaces during the treatments. High surface free energy core anchoring of less stable metal shells appears to be a valid strategy extendable to many other systems.

Keywords: Strong Electrostatic Adsorption; Electroless Deposition; core-shell particle stabilization; gold catalysis

1 Introduction

The sintering of supported metal catalysts and the corresponding loss of active surface sites is perhaps the most common cause of catalyst deactivation. Attempts to minimize sintering include synthesizing particles of monodisperse size [1], increasing the density of support defects, for example by employing a form of cerium oxide with ample step sites to anchor individual Pt ions as PtO_4 [2] or doping carbon with nitrogen, which can form metal-N bonds [3], by adding a promoter such as lanthanum to anchor Pd atoms [4], by overcoating metal nanoparticles with carbon [5] or an atomic layer deposited coating of silica or alumina [6], or with a one pot synthesis which surrounds metal nanoparticles with a shell of oxide [7].

A particularly challenging reactive condition is the severely corrosive environment of concentrated gaseous hydrogen chloride at elevated temperature as occurs in acetylene hydrochlorination. In previous work, it was demonstrated that while 1.5 nm Au nanoparticles supported on carbon were stable in an inert carrier gas at 180°C and 1 atm, sintering to large particles (10-20nm) occurred within minutes when the Au catalysts were exposed to a 50% HCl in He mixture, or to a reaction stream of 32% acetylene, 32% HCl, and balance He, at the same temperature and pressure [8].

Efforts to prevent Au sintering in gaseous HCl environments have included the applications of ionic liquids [9,10], the addition of sulfur or nitrogen-containing ligands [11], or doping the carbon support with nitrogen [12]. Most strategies using a second metal in the synthesis of Au catalysts such as Cu, Cs, Ba, Li, Bi, and Sr are aimed at promoting the Au and increasing the activity in the hydrochlorination reaction. A number of bimetallic catalysts including gold alloyed with copper, bismuth or nickel [13-16] have been prepared by co-impregnation in which the bimetallic nanoparticle morphology was

not well controlled nor well characterized. These efforts have had limited success in the prevention of sintering; several have reduced the extent of sintering [17-21] but none have eliminated it.

In the present work we wish to demonstrate a simple, generalizable method to stabilize supported metals, using Au in an HCl environment as an example, by selectively placing the metal as a shell on a core of higher surface free energy (SFE) metal which is stable in the particular thermochemical environment. In principle, the thermodynamic driving force to minimize SFE will keep the shell metal on the core metal and off the lower SFE support, so stabilizing the shell metal against sintering.

This hypothesis can be applied and tested with very well dispersed core-shell particles. First, strong electrostatic adsorption (SEA) can be used to synthesize ultrasmall (< 2 nm) supported nanoparticles with a variety of metals on a variety of oxide and carbon [22-24] supports. Subsequently, sub-, mono-, and multi-layers of a second metal shell can be deposited on the metal core by electroless deposition (ED), which itself has been demonstrated for a wide variety of core metal/shell metal pairs [25]. Electroless deposition of Au using a well-studied gold deposition developer bath [26, 27] has been demonstrated for a number of metal cores to produce well-characterized bimetallic catalysts having core-shell structures at various Au metal coverages [28].

Shells of gold, the SFE of which is 1.626 J/m^2, might be stabilized by cores of ruthenium or platinum which have SFEs of 3.409 J/m^2 and 2.691 J/m^2, respectively [29,30] and should not migrate to the low SFE carbon support (0.506 J/m^2). Thus, it should be thermodynamically favorable for gold atoms to cover the higher surface energy core metal and exist as a thin shell, reducing the overall SFE of the system. Provided that Ru and Pt nanoparticles are themselves stable in the reaction environment, stabilized Au cores on

ultra-small (< 2 nm) cores will result in a stable core-shell nanoparticle with high utilization of the Au.

Nanoparticle stability was tested in a He/HCl mixture as well as a He/HCl/acetylene mixture typical of acetylene hydrochlorination. We characterized the core-shell nanoparticle size with both powder XRD and high aberration-corrected, high resolution scanning transmission microscopy. The coverage of Ru and Pt cores by Au shells is confirmed with selective chemisorption and high resolution elemental mapping in the electron microscope. Pt and Ru nanoparticles are shown to be stable on carbon in the corrosive environment, and these core metals are seen to completely stabilize the Au shells in the sintering environment.

2 Experimental

2.1 Supported nanoparticle preparation via SEA

One weight percent carbon-supported Au nanoparticles used in this study were synthesized by electrostatic adsorption of bis(ethylenediamine)gold(III)chloride [$Au(en)_2Cl_3$] onto Darco KBB carbon with BET surface area of 1500 m^2/g. The point of zero charge (PZC) was measured to be 4.8. The $Au(en)_2Cl_3$ was synthesized according to the method of Block and Bailar [31]. A standard solution of 160 ppm Au was prepared by dissolving freshly prepared $Au(en)_2Cl_3$ in deionized water. A metal uptake survey was conducted to determine the pH of optimal metal uptake with precursor solutions containing 160 ppm of Au and the pH was adjusted over the range of 1-13, using 40 ml of this gold solution and an amount of carbon to 1000 m^2 carbon/L of solution. This constant surface loading ensured a similar number of surface sites at all pH shift experiments.

$$\text{Surface loading } \left(\frac{m^2}{L}\right) = \frac{\text{Surface Area of support } \left(\frac{m^2}{\text{g}}\right) * \text{grams of support(g)}}{\text{volume of precursor solution (L)}} \quad \text{(Equation 1)}$$

Samples were stirred for 60 minutes before filtering and reserving a 10 ml aliquot of the contacted solution. The Au concentration was measured and compared to the parent solution using a Perkin Elmer Optima 2100 DV ICP-OES. Adsorption amounts were calculated using Equation 2 and are expressed as micromoles of Au per square meter of support. The optimal pH (pH of greatest metal uptake) was used to scale to give two grams of material. The finished samples were filtered and vacuum dried at 25°C for 24 hours before being reduced in flowing 10% H_2/He for 60 minutes at 150°C.

$$\text{Uptake } \Gamma \left(\frac{\mu\text{mol}}{\text{m}^2}\right) = \left(\text{C}_{\text{inital}} \left(\frac{\text{mg}}{\text{L}}\right) - \text{C}_{\text{final}} \left(\frac{\text{mg}}{\text{L}}\right)\right) * \frac{10^6 \left(\frac{\mu\text{mol}}{\text{mol}}\right)}{\text{surface loading } \left(\frac{\text{m}^2}{\text{L}}\right) * \text{M.W.of metal } \left(\frac{\text{g}}{\text{mol}}\right) * 1000 \frac{\text{mg}}{\text{g}}}$$

(Equation 2)

Uptake surveys and scaled-up syntheses of Ru and Pt were also similarly performed to give loadings of 0.5 wt% Ru and 1.0 wt% Pt, resulting in similar molar loadings of Au, Ru, and Pt. Tetraammine platinum(II) chloride (PTA), and hexaammine ruthenium(II) chloride ($RuHA^{2+}$) were used as metal salts for preparation of the monometallic systems. Synthesis of these low PZC supported nanoparticles using SEA methods have been previously published [32-34] and have been shown to produce highly dispersed metal crystallites. The reduction temperatures employed for the monometallic Au, Ru, and Pt nanoparticles were determined by TPR to be 150, 250, and 250ºC, respectively.

2.2 Core-shell nanoparticle preparation via electroless deposition

A series of carbon supported Pt@Au/C and Ru@Au/C bimetallic nanoparticles were prepared by the electroless deposition of $KAu(CN)_2$ using hydrazine (N_2H_4) as the reducing agent. M@Au denotes a shell of Au deposited on the core metal M. The initial

molar ratio of N_2H_4 to Au salt in the bath was maintained at N_2H_4 : $KAu(CN)_2$ = 10 : 1 for all preparations. The electroless developer bath volume was 200 ml and 0.5 g of either the 0.5 wt% Ru or 1.0 wt% Pt/C was used as substrate for gold deposition. Deposition experiments were conducted at 40°C by placing the beaker for ED in a temperature-controlled oil bath. Initial pH of the baths was adjusted to pH 10 with concentrated NaOH and pH was monitored and maintained at pH 10 during deposition. Due to the low PZC carbon at 4.8, there was no adsorption of $Au(CN)_2^-$ on the support. Depositions were carried out for 180 minutes to ensure complete deposition of $Au(CN)_2^-$. Samples were then washed with 2L of DI H_2O to ensure removal of residual ligands and salts, then filtered and dried overnight at room temperature before storage at ambient conditions. Blank experiments were conducted to confirm that a solution of N_2H_4 and $KAu(CN)_2$ at pH 10 did not undergo thermal reduction or deposit on the carbon support, consistent with results for other similar systems [26, 27].

2.3 Nanoparticle stability treatments

Supported nanoparticles were treated in a fixed bed, Pyrex reactor (3/8" OD) in a either in a mixture of 50% He diluent and 50% anhydrous HCl gas (Praxair, 99.999%) using 20 SCCM of gas flow at 180°C for 1 hour, which are termed "aged" samples, or in a gas mixture representative of acetylene hydrochlorination (He : C_2H_2 : HCl ratio = 1.0 : 1.0 : 1.1 at 180°C and total flow of 31 SCCM), which are referred to as "spent" samples. In the latter treatment the C_2H_2 was run through a bed of molecular sieve 5A to remove the acetone inhibitor prior to mixing with He and HCl. Prior to the start of either sintering treatment the samples were reduced *in situ* reduction for 1 hour in flowing 10% H_2/balance He at 30 SCCM.

2.4 Supported nanoparticle characterization

Powder X-Ray diffraction (XRD) was used to investigate the crystalline characteristics of the supported metal nanoparticles; particle size was determined by the Scherrer equation. The XRD patterns were obtained with a Rigaku Miniflex-II equipped with a high sensitivity D/Tex Ultra detector. The radiation source was Cu-Kα radiation (λ = 1.5406 Å) operated at 30kV and 15mA. All patterns were taken at a scan rate of 0.5°/min and sampling width of 0.02° over the 2θ range of 20-80°. An advanced x-ray detector, such as the D/TeX ultra, can provide data with an excellent signal to noise ratio and are accurate for particle size determinations as low as 1.5 nm for well-defined carbon-supported systems [35].

The amount of Au salt remaining in solution as a function of deposition time for the ED gold developer bath was measured by atomic absorption spectroscopy (PerkinElmer AAnalyst400). The amount of gold deposited on the monometallic substrate was used to determine the theoretical surface coverage of Au on the core metal, assuming monodisperse coverage of Au on Pt or Ru (1:1 atomic ratio). The metal concentrations for each monometallic sample prepared via SEA (Ru, Pt and Au) was measured by inductively coupled plasma-optical emission spectroscopy (ICP-OES) on a Perkin Elmer Optima 2100DV.

For chemisorption measurements, Pt/C, Ru/C, and bimetallic M@Au/C nanoparticles were characterized using H_2 titration of oxygen pre-covered Pt or Ru sites using a Micromeritics AutoChem 2920 Automated Analyzer. Samples were reduced at 200°C or 250°C, for Pt and Ru nanoparticles, respectively, at a heating rate of 10°C/min in 10% H_2/Ar and held at the final temperature for 1 hr**.** Samples were then purged in flowing Ar for 30 min at 200°C or 250°C before cooling to 40°C. A 10% O_2/Ar mixture was then

flowed over the material for 30 min to saturate the surface with chemisorbed oxygen before purging in Ar for 10 min to remove residual, gas phase O_2. The samples were then dosed with a known volume (0.518 cm^3) of 10% H_2/Ar until all Pt-O surface sites had been removed to form H_2O and Pt-H, giving an adsorption stoichiometry of 1.5 H_2/Pt site. For Ru, titration of Ru-O_2 sites (geminal O atoms on Ru) formed 2 H_2O + Ru-H based on previous work, to give an adsorption stoichiometry of 2.5 H_2/Ru site [36]. Consumption of H_2 was quantitatively determined with a high sensitivity, thermal conductivity detector downstream from the sample cell. Fractional coverage $\theta_{(Au)}$ of Au on Pt was determined by the difference of H_2 uptakes for the monometallic Pt/C and the Pt@Au compositions. Likewise, $\theta_{(Au)}$ of Au on Ru was determined from the difference of H_2 uptakes for the monometallic Ru/C and the Ru@Au compositions, since Au is not active for either O_2 or H_2 chemisorption at 40°C. Similar arguments have been used to calculate the coverage of Pt or Pd surface atoms by Au [27, 37-39].

STEM and EDXS analysis were performed using a JEM-ARM200CF for both fresh, aged (in HCl) and spent (after prolonged exposure to HCl and C_2H_2 reaction feeds) samples. The JEM-ARM200CF is a probe aberration-corrected 200kV TEM with a cold field emission source and a 0.35 eV resolution. The microscope is also equipped with an Oxford X-max 80 SDD X-ray detector with a probe size of one angstrom and a current of 14 Pa, 20μ. Maps were generated within 5 minutes to help ensure the core-shell structure remained intact.

3 Results and Discussion

3.1 Preparation of supported monometallic nanoparticles

The uptakes of $Au(en)_2^{3+}$, PTA^{2+}, and $RuHA^{2+}$ on carbon as a function of final pH are plotted in Figure 1. Typical volcano shaped curves were observed, which is an indication of electrostatic adsorption of the metal complexes on the support surface [20, 39, 40]. Maximum uptake of metal occurs at final pH values of 10 - 12 with an uptake of 0.79 μmol/m^2 for $Au(en)_2^{3+}$, 0.82 μmol/m^2 for $RuHA^{2+}$, and 0.71 μmol/m^2 for PTA^{2+}.

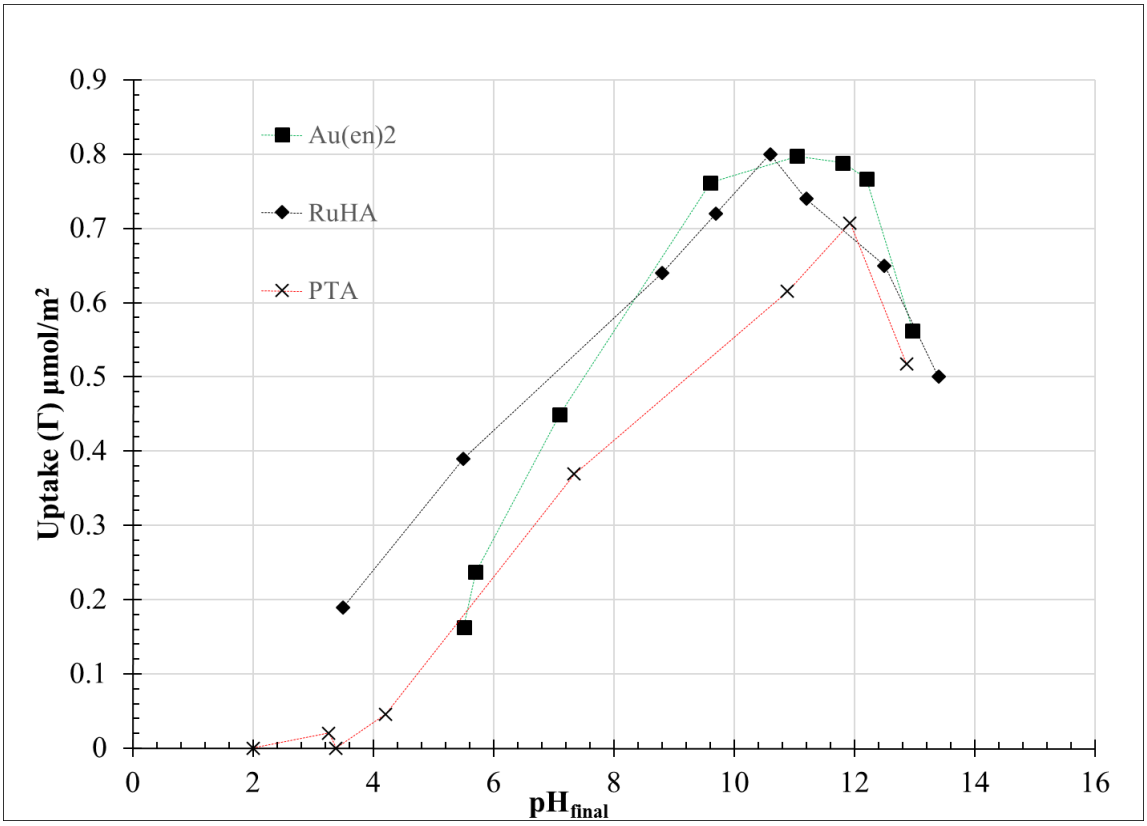

Figure 1. Uptake of Au, Pt, and Ru over 1000 m^2/L carbon as a function of the final pH of the adsorption solution.

Metal adsorption decreases at higher pH as the ionic strength of the adsorption solution increases which reduces the adsorption equilibrium constant due to double layer screening [24]. At low pH values near the PZC of the carbon support the uptake is also low, since the

surface charge of the support is minimal and the charge difference between the metal complex and support surface is the driving force for electrostatic adsorption [24].

Thus, sufficiently large quantities of monometallic Au, Ru, and Pt samples were synthesized at optimal pH values of 11.8, 10.5 and 12.0, respectively. The XRD characterization of these materials is shown in Figure 2a. The absence of hcp peaks for Ru indicates very small particle sizes, below the approximately 1.5 nm limit of detection of the diffractometer. In the case of Pt, very broad fcc peaks were observed; after careful deconvolution from the background [35], the average size was determined to be 1.8 nm. Small particle sizes for both metals are further confirmed by STEM images, shown in Figure 3. Not only are the metal particles small, each sample also contains a significant fraction of isolated atoms.

The stability of these three samples in HCl at the reaction temperature and in the condition of hydrochlorination of C_2H_2 was examined next. To test particle growth in anhydrous HCl, samples were dried at 180°C for 1 hour in 10 SCCM He to remove water and then exposed at 180°C to a total flow of 20 SCCM at a 1:1 ratio of HCl : He for 1 hour. The system was then purged with N_2 and cooled to room temperature and the samples were removed for XRD analysis. These XRD results are shown in Figure 2b, and the size estimates are summarized in Table 1. The Pt/C sample showed no detectable peak sharpening; the peak width again indicated an average particle size of 1.7 nm. The Ru/C

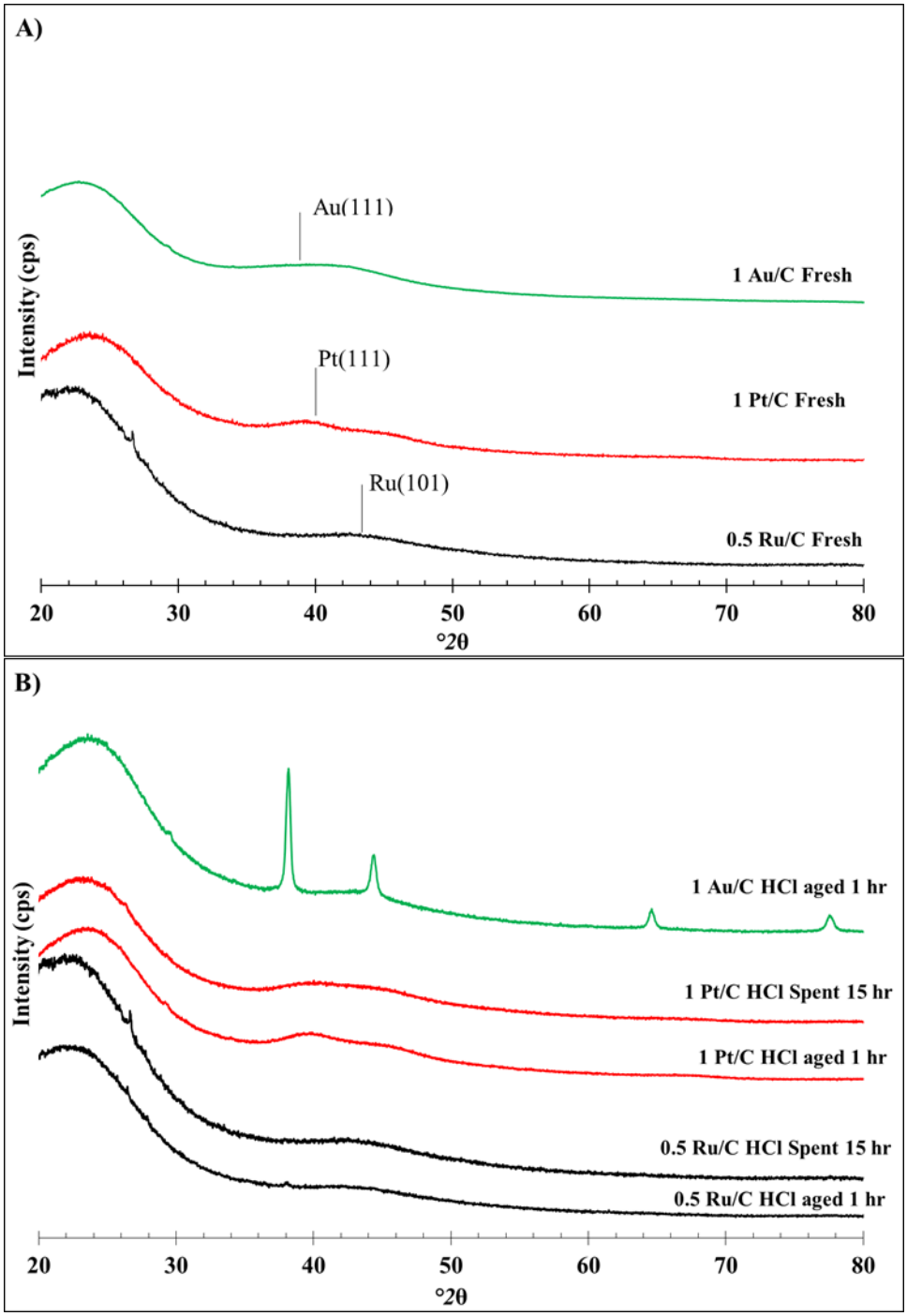

Figure 2. XRD patterns for all freshly prepared SEA catalysts after reduction (A) and after exposure to HCl : He = 1:1 (20 SCCM flow) at 180°C for one hour and (B) after pretreatment and reaction in HCl : He : C_2H_2 = 1.1:1.0:1.0 at 180°C for 15 hours. Positions of primary peaks are Au(111) = 38.25°, Pt(111) = 39.76°, and Ru(101) = 44.18°.

displayed no perceptible increase in peak sharpening after HCl exposure. As reported previously [8], Au sintered significantly after 5 minutes of HCl exposure and only

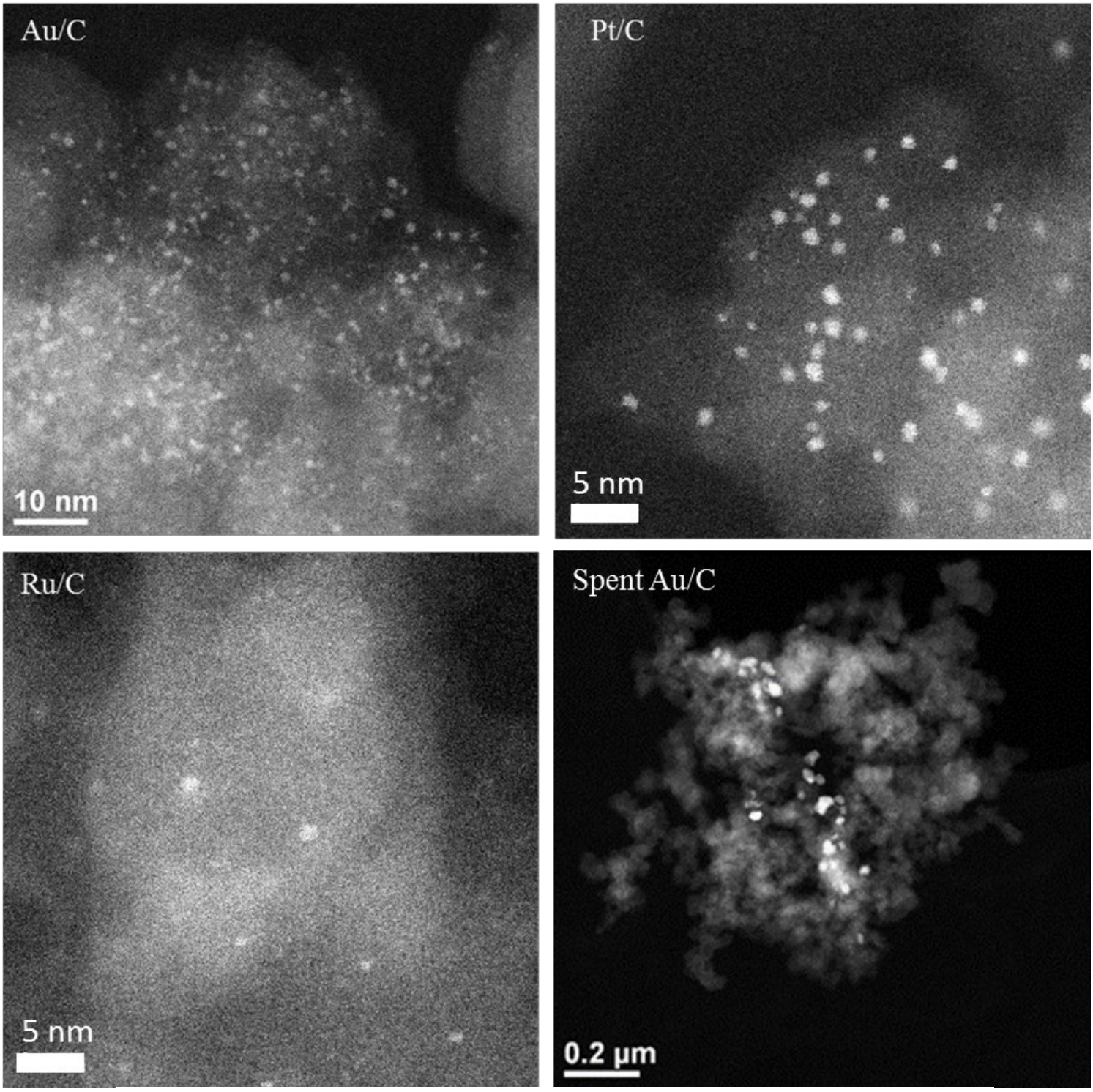

Figure 3. STEM of fresh Au, Ru and Pt/C and a spent Au/C catalyst.

marginally more after an additional 100 hours (Table 1). This is also shown in the micrograph of the aged Au sample of Figure 3 and agreed with XRD analysis. The Au/C

sample in Figure 2a was exposed to flowing He for one hour at 180ºC and no Au particle sintering occurred as observed previously [8]. Thus, it is the chemical environment and not the temperature that causes Au particles to sinter. In the same environment, Ru and Pt are thoroughly resistant to sintering.

Table 1. Summary of metal particle size as a function of time in HCl for Au/C, Pt/C and Ru/C. Data for 1 wt% Au/C taken from [8].

Sample	**Initial particle size from XRD, (nm)**	**Time in HCl flow, (min)**	**Final particle size from XRD, (nm)**
1 wt. % Au/C	<1.5	5	20.6
1 wt. % Au/C	<1.5	15	18.8
1 wt. % Au/C	<1.5	45	20.4
1 wt. % Au/C	<1.5	60	20.7
1 wt. % Au/C	<1.5	1200	19.5
1 wt. % Au/C	<1.5	6000	22.2
0.5 wt. % Ru/C	<1.5	60	<1.5
0.5 wt. % Ru/C	<1.5	900	<1.5
1 wt. % Pt/C	1.8	60	1.7
1 wt. % Pt/C	1.8	900	<1.5

For long term aging under reaction conditions, the single metal samples were dried and pre-chlorided in the same fashion as before after which they were aged in a mixture of He, C_2H_2, and HCl in a ratio of 1.0:1.0:1.1 at 180°C and total flow of 31 SCCM. The samples were aged for 15 hours and then thoroughly purged and cooled before removal. The post-treatment XRD patterns in Figure 2b reveal that the Ru and Pt samples were also completely stable with respect to sintering. Au, on the other hand, sintered rapidly and markedly in the gaseous HCl [8].

Preparation and Stability Evaluation of Core-Shell Bimetallic Nanoparticles

Bimetallic nanoparticles were prepared using ED to deposit controlled amounts of Au on the surface of both core metals. Potassium dicyanoaurate, $KAu(CN)_2$ was used in all cases as the gold metal salt for deposition onto the highly dispersed Pt and Ru core metals to give theoretical coverages of 1 and 2 monodisperse Au layers. These values were chosen to maintain Au weight loadings similar to those used by others [13].

Electroless deposition of Au was conducted at pH 10 using hydrazine as the reducing agent at an initial 10:1 molar ratio of N_2H_4 to $Au(CN)_2^-$. Concentrations of $Au(CN)_2^-$ remaining in the ED bath were monitored by atomic absorption at different time intervals over 180 min to ensure complete gold deposition. Figure 4a shows plots for the kinetics of Au deposition on Pt at 1.0 and 2.0 theoretical monolayers (MLs) of Au. A control experiment at pH 10 with no N_2H_4 in the ED bath was performed to ensure there was no electrostatic adsorption of $Au(CN)_2^-$. For Au deposition, a N_2H_4 solution at pH 10 was added to the pH 10 bath containing $KAu(CN)_2$; the Pt/C or Ru/C core nanoparticles were added 30 minutes later. The stability of the bath during this initial 30 min period confirmed the bath was thermally stable with respect to spontaneous reduction.

At initial Au^+ (as $KAu(CN)_2$) concentrations of 13 and 25 ppm, the deposition of 1.0 and 2.0 theoretical MLs of Au on Pt was completed within 70 and 120 minutes, respectively. Since the control run with carbon only demonstrated that electrostatic adsorption of $Au(CN)_2^-$ on carbon did not occur, only ED occurred as either catalytic

deposition on Pt and/or autocatalytic deposition onto freshly deposited Au. Deposited Au

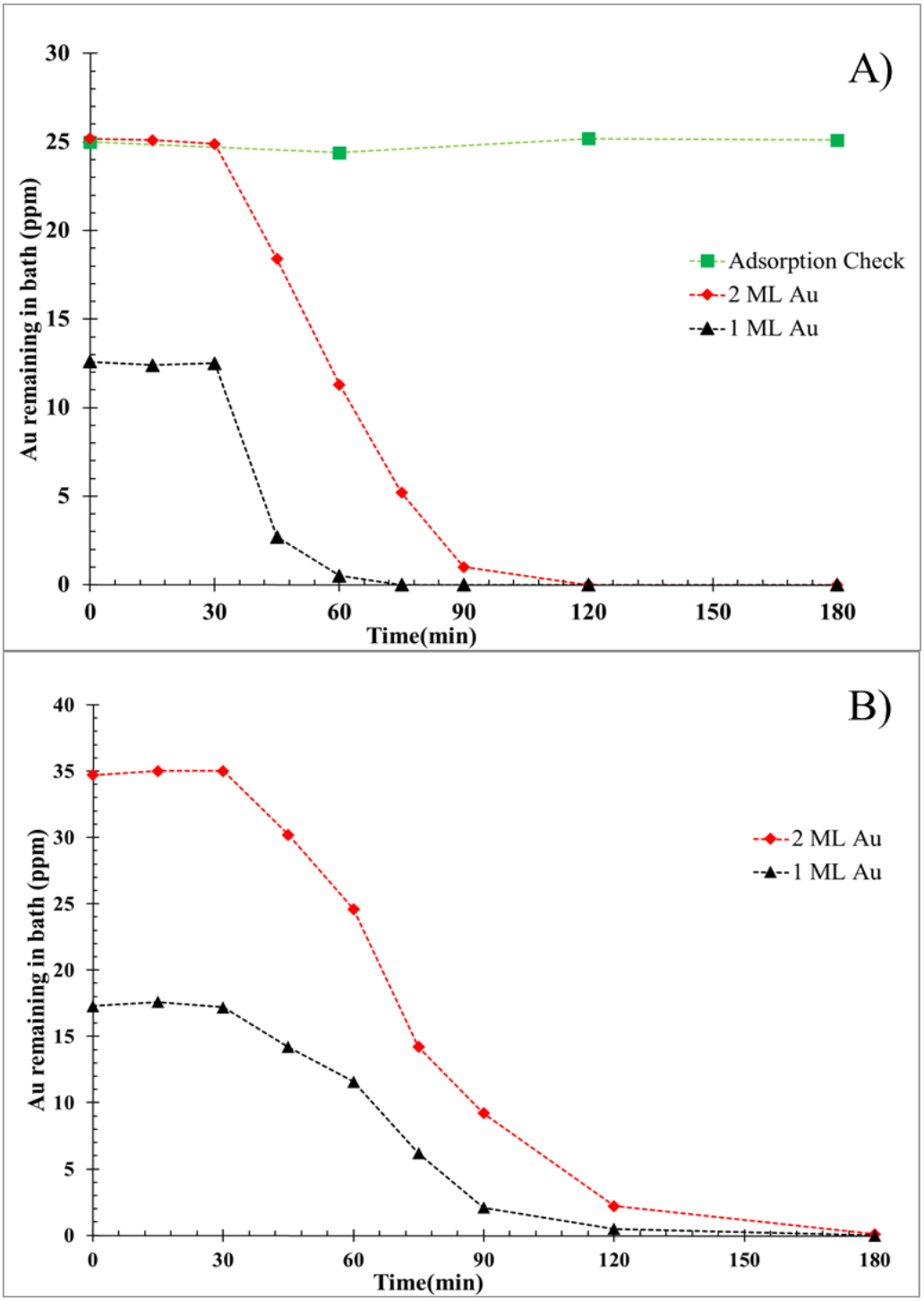

Figure 4. Concentration of Au^{+} remaining in ED bath as a function of time for deposition of nominal coverages of 1.0 and 2.0ML Au on (a) 1.0 wt% Pt/C, and (b) 0.5 wt% Ru/C. Addition of monometallic catalyst occurred 30 minutes after start of experiment. The SEA adsorption check in (a) confirms $Au(CN)_2^-$ was not adsorbed on the C surface.

weight loadings were calculated to be 0.47 and 0.95 wt. % for the nominal 1.0 ML and 2ML coverages.

Figure 4b illustrates the deposition of 1.0 and 2.0 theoretical ML of Au on 0.5 wt. % Ru/C. Deposition of Au occurred more slowly for Ru compared to Pt, requiring 180 minutes for both loadings. Calculations for 1.0 and 2.0 ML coverages corresponded to 0.51 wt. % and 1.02 wt. % Au, respectively. The slower kinetics suggest that activation of N_2H_4 on Ru occurs more slowly than on Pt surfaces.

The bimetallic Pt@Au/C and Ru@Au/C samples were characterized by chemisorption to experimentally determine the Au coverages on Pt and Ru and the results are shown in Table 2. Gold coverages were determined by the decrease in H_2 uptake compared to the monometallic Pt and Ru samples, since Au is inactive for H_2 titration of O-precovered sites at these conditions [38, 39]. The lower H_2 uptake values for Pt and Ru surface sites after the deposition of Au confirmed deposition to form core@shell structures. From chemisorption analyses, 1.0 and 2.0 theoretical ML coverages of Au on 1.0 wt% Pt corresponded to experimental coverages of 0.55 and 0.85 ML Au, respectively. For similar Au coverages on 0.5 wt% Ru, chemisorption analyses gave 0.25 and 0.53 ML Au coverage on Ru. Chemisorption analyses of the 2.0 ML samples after 15 h of reaction showed that Au coverages had increased from 0.85 to 0.96 ML for the Pt@Au sample and from 0.53 to 0.94 for Ru@Au, suggesting that Au had spread on the Pt and Ru surfaces during reaction. This may indicate that the lower surface free energy (SFE) value of Au relative to Pt or Ru caused surface diffusion of Au to cover more of the higher SFE surfaces of Pt and Ru during reaction. All the experimental Au coverages were lower than theoretical coverages, indicating that in addition to catalytic deposition of Au on Pt or Ru autocatalytic deposition of Au on Au sites also occurred. This indicated that multi-layer structures of Au existed

on the surfaces of the core metals. Autocatalytic deposition of Au has also been observed in previous studies for bimetallic, Au-containing compositions [27, 28]. This was more pronounced for Au deposition on Ru, suggesting again that Ru is less active than Pt for activation of N_2H_4, indicating that activation of N_2H_4 on Au competed more favorably and autocatalytic deposition of Au was more pronounced. That the spent samples of both Pt and Ru were converging to the same, increased fractional coverage is an indication that surface thermodynamics is prevailing over the initial kinetics of ED.

Table 2. Summary of fractional coverage determined via chemisorption for (Pt@Au and Ru@Au bimetallic samples.

Theoretical coverage of Au (ML)	**Au wt. loading (wt %)**	**H_2 uptake (cm^3/g)**	**Fractional coverage of Au**
	(on 1 wt% Pt/C)		
0.0	0	4.85	0
1.0	0.47	2.17	0.55
2.0	0.95	0.73	0.85
2.0 spent	0.95	0.20	0.96
	(on 0.5 wt% Ru/C)		
0.0	0	6.48	0
1.0	0.51	3.04	0.25
2.0	1.02	2.72	0.53
2.0 spent	1.02	0.16	0.94

XRD characterization of fresh and reaction-aged (spent) 1 and 2 ML Au shells on Ru and Pt cores is shown in Figure 5. The patterns for the fresh materials, which contain almost no evidence of crystalline Au, except for the presence of a very small Au (111) peak for the spent 1ML and 2 ML Ru@Au samples in the top half of Figure 5. The intensity of these barely perceptible peaks is less than one-half of one percent of the intensity of the Au peak of the sintered sample in Figure 2. The fresh samples free of Au peaks further suggest

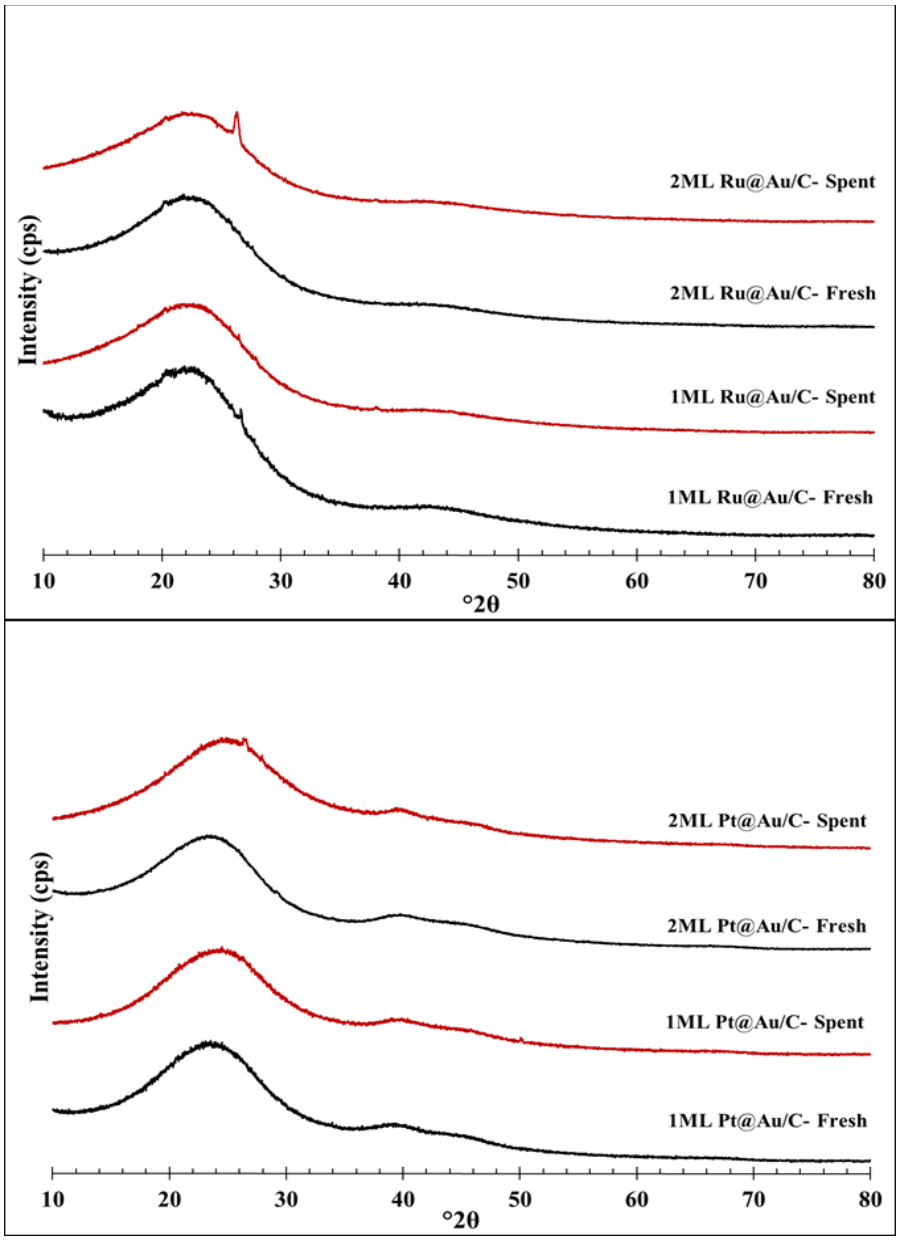

Figure 5. XRD patterns for Ru@Au/C and Pt@Au/C materials both before (fresh) and after (spent) 15 h on-line for C_2H_2 hydrochlorination. Au(111) peak position is 38.25°. For spent materials, small peak at 26° is NaCl resulting from reaction of Na impurity in C and HCl during treatment.

that autocatalytic deposition of Au did not occur to a high extent. Of course, if deposition of Au was primarily restricted to 1 – 3 atom-thick layers of Au on Pt and Ru surfaces, the Au would likely appear amorphous for XRD. In fact, the patterns of the nominal 1.0 and

2.0 ML loadings of Au on both Ru and Pt cores in Figure 5 appear identical to the single metal diffraction profiles of the fresh samples seen in Figure 2.

In the XRD characterization of reaction-treated (spent) samples in Figure 5, fcc Au peaks are also wholly absent, unlike the post-reaction monometallic Au sample in Figure 2 which exhibited very sharp Au peaks corresponding to particles of 20 nm average size. The absence of Au peaks in the spent core-shell nanoparticles in Figure 5 indicates a remarkable stability of the Au in these core-shell nanoparticles, even at 1:1 atomic ratio with the core metals; the high surface free energy cores of Ru and Pt appear to completely anchor the Au against sintering in the reactive HCl environment. In fact, chemisorption results of the spent materials, given in Table 2, reveal further blockage of Pt and Ru in the spent samples by the Au shells. The coverage of the 2 ML samples increased to 0.94 and 0.96 monolayers, from pre-treatment values of .85 and .53 monolayers. This decrease is consistent with the further spreading of autocatalytically-deposited Au during the reaction, though it may also be due to Pt and Ru site blockage by coke as acetylene may interact strongly with the exposed Ru and Pt atoms [40, 41].

To this point, XRD has revealed that no Au sintering occurs, and chemisorption indicates that the Pt and Ru surfaces are blocked, presumably by Au shells, with some spreading of Au shells after aging. To complement these two sets of results, a final direct characterization of the location of the Au and Pt was made with STEM elemental mapping. Atomically resolved images of the post-reaction Pt@ 2 ML Au materials are given in Figure 6. Besides the sub-2 nm crystallites, individual and paired metal atoms are readily observable. Images of the reactant-treated samples were virtually unchanged from fresh samples. The size of the nanoparticles of about 2 nm agrees with the value obtained from

XRD (Table 1) of 1.7 nm. (Pre- and post-treated Ru@Au samples were also unchanged in morphology and showed almost no crystallinity and EDXS maps are inconclusive [42].) Most importantly, the Pt and Au maps on the right of Figure 6 show that Au is associated with each Pt nanoparticle. It is noted that the three nanoparticles in the maps are colinear whereas in the image on the left, they are not. This was due to the sample being slightly tilted to optimize the collection of x-rays. The single pixels in the rest of the maps are noise. Consistent with XRD, there was no observation of any sintered Au in either the Pt or Ru-core samples.

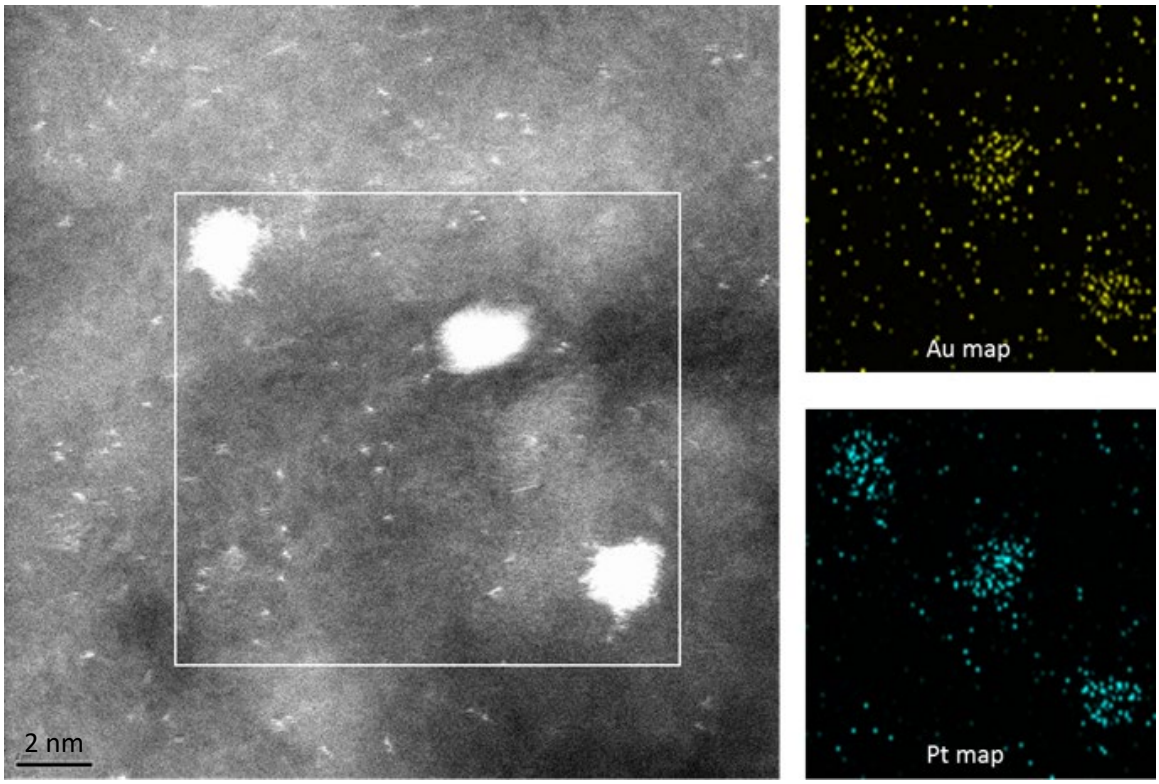

Figure 6. STEM images of 2ML Au over Pt after reaction; EDXS maps of Au and Pt on the right.

The STEM characterization is the final necessary piece of this characterization puzzle; XRD shows that Au shells deposited on Pt or Ru cores have not sintered in the

corrosive environment as does the same mass of Au in the form of single metal nanoparticles; chemisorption shows that the surfaces of Pt and Ru core particles are blocked and become more blocked with aging in HCl or HCl/C_2H_2; and STEM shows that Au and Pt domains are co-located and are about the same diameter. These three characterizations can be quite reasonably interpreted with a model of Au shells on Pt or Ru cores. That the Au exists in shells and not dissolved into the Pt or Ru crystal lattices is suggested by the severity of chemisorption blockage, which becomes more pronounced with aging. Such a high degree of blockage would not likely occur if a significant portion of the Au were dissolved into the Pt or Ru nanoparticle cores.

While the acetylene hydrochlorination reaction environment has provided an excellent test of stabilizing nanoparticles of Au, the activity of these catalytic materials is not in fact dependent on nanoparticulate, metallic Au. The most recent literature [43-45] and particularly EXAFS and XANES [45] have been used to demonstrate that the active sites for this reaction are isolated Au ions in close contact with a carbon surface. Our own prior work [8] showed that oxide supports over which small Au nanoparticles were stable under the reaction conditions gave almost no activity, and carbon supports over which isolated atoms exist were active (but slowly deactivated). Isolated Au can be stabilized and promoted by soft ligands such as thiosulfate and thiocyanate [43,46]. The acetylene hydrochlorination activity of the Pt/Au and Ru/Au materials in the present study does become stable and likely involves the stabilization of Au atoms, and has been reported separately [42] as the focus here is on the stabilization of metal shells by high surface free energy metal cores.

4 Conclusion

The coupling of SEA with ED gives an unprecedented degree of control for both particle dispersion and morphology of core-shell particles. Carbon supported gold nanoparticles which sinter heavily in concentrated HCl and HCl/acetylene gases at elevated temperature were completely stabilized in these environment via anchoring the Au onto high surface free energy metal cores. These metal cores, prepared via SEA, can be synthesized with a high degree of dispersion and monodispersity, and the shells prepared at precisely controlled weight loadings. The ability to stabilize gold surfaces in harsh chemical environments using high SFE core can certainly be applied to other reactions in less severe environments but in which gold nanoparticles are known to sinter such as water-gas shift or low temperature CO oxidation.

Conflicts of Interest

There are no conflicts of interest to declare.

Acknowledgements

The authors would like to acknowledge the following NSF grant numbers: IIP1464630 and CBET1511615.

References

[1] C.E. Pompe, M. Slagter, P.E. De Jongh, K.P. De Jong, Impact of Heterogeneities in Silica-Supported Copper Catalysts on Their Stability for Methanol Synthesis. J. Catal. 2018, 365, 1–9.

[2] D. Kunwar, S. Zhou, A. Delariva, E.J. Peterson, H. Xiong, X.L. Pereira-Hernández, S.C. Purdy, R. Ter Veen, H.H. Brongersma, J.T. Miller, A.K. Datye, et al. Stabilizing High Metal Loadings of Thermally Stable Platinum Single Atoms on an Industrial Catalyst Support. ACS Catal. 2019, 9 (5), 3978–3990.

[3] S. Tian, Q. Fu, W. Chen, Q. Feng, Z. Chen, J. Zhang, W. Cheong, R. Yu, L. Gu, J. Dong, Y. Li, et al. Carbon Nitride Supported Fe2 Cluster Catalysts with Superior Performance for Alkene Epoxidation. Nat. Commun. 2018, 9 (2353), 1–7.

[4] J.R. Gaudet, A. De La Riva, E.J. Peterson, T. Bolin, A.K. Datye, Improved Low-Temperature CO Oxidation Performance of Pd Supported on La-Stabilized Alumina. ACS Catal. 2013, 3 (5), 846–855.

[5] H.N. Pham, A.E. Anderson, R.L. Johnson, T.J. Schwartz, B.J. O'Neill, P. Duan, K. Schmidt-Rohr, J.A. Dumesic, A.K. Datye, Carbon Overcoating of Supported Metal Catalysts for Improved Hydrothermal Stability. ACS Catal. 2015, 5 (8), 4546–4555.

[6] H. Zhang, C. Canlas, A. Jeremy Kropf, J.W. Elam, J.A. Dumesic, C.L. Marshall, Enhancing the Stability of Copper Chromite Catalysts for the Selective Hydrogenation of Furfural with ALD Overcoating (II) - Comparison between TiO2 and Al2O3 Overcoatings. J. Catal. 2015, 326, 172–181.

[7] K. Wu, X.Y. Wang, L.L. Guo, et al., Facile synthesis of Au embedded CuO_x-CeO_2 core/shell nanospheres as highly reactive and sinter-resistant catalysts for catalytic hydrogenation of p-nitrophenol. Nano Res. 202013**,** 2044–2055.

[8] K.C. O'Connell, J.R. Monnier, J.R. Regalbuto, The Curious Relationship of Sintering to Activity in Supported Gold Catalysts for the Hydrochlorination of Acetylene. Appl. Catal. B Environ. 2018, 225 (December 2017), 264–272.

[9] J. Zhao, Y. Yu, X. Xu, S. Di, B. Wang, H. Xu, J. Ni, L.L. Guo, Z. Pan, X. Li, Stabilizing Au(III) in Supported-Ionic-Liquid-Phase (SILP) Catalyst Using CuCl2 via a Redox Mechanism. Appl. Catal. B Environ. 2017, 206, 175–183.4

[10] J. Zhao, S. Gu, X. Xu, T. Zhang, Y. Yu, X. Di, J. Ni, Z. Pan, X. Li, Supported Ionic-Liquid-Phase-Stabilized Au(III) Catalyst for Acetylene Hydrochlorination. Catal. Sci. Technol. 2016, 6 (9), 3263–3270.

[11] H. He, J. Zhao, B. Wang, Y. Yue, G. Sheng, Q. Wang, L. Yu, Z.T. Hu, X. Li, Highly Active AuCu-Based Catalysts for Acetylene Hydrochlorination Prepared Using Organic Aqua Regia. Materials (Basel). 2019, 12 (8).

[12] J. Zhao, T. Zhang, X. Di, J. Xu, J. Xu, F. Feng, J. Ni, X. Li, Nitrogen-Modified Activated Carbon Supported Bimetallic Gold-Cesium(I) as Highly Active and Stable Catalyst for the Hydrochlorination of Acetylene. RSC Adv. 2015, 5 (9), 6925–6931.

[13] M. Conte, A.F. Carley, G. Attard, A.A. Herzing, C.J. Kiely, G.J. Hutchings, Hydrochlorination of acetylene using supported bimetallic Au-based catalysts, Journal of Catalysis, 257 (2008) 190-198

[14] K. Zhou, J. Jia, X. Li, X. Pang, C. Li, J. Zhou, G. Luo, F. Wei, Continuous vinyl chloride monomer production by acetylene hydrochlorination on Hg-free bismuth catalyst: From lab-scale catalyst characterization, catalytic evaluation to a pilot-scale

trial by circulating regeneration in coupled fluidized beds, Fuel Processing Technology, 108 (2013) 12-18.
[15] K. Zhou, W. Wang, Z. Zhao, G. Luo, J.T. Miller, M.S. Wong, F. Wei, Synergistic Gold–Bismuth Catalysis for Non-Mercury Hydrochlorination of Acetylene to Vinyl Chloride Monomer, ACS Catalysis, 4 (2014) 3112-3116.
[16] S. Wang, B. Shen, Q. Song, Kinetics of acetylene hydrochlorination over bimetallic Au–Cu/C catalyst, Catalysis letters, 134 (2010) 102-109.
[17] J. Zhao, J. Xu, J. Xu, J. Ni, T. Zhang, X. Xu, X. Li, Activated-Carbon-Supported Gold-Cesium(I) as Highly Effective Catalysts for Hydrochlorination of Acetylene to Vinyl Chloride. Chempluschem 2015, 80 (1), 196–201.
[18] H. Zhang, W. Li, X. Li, W. Zhao, J. Gu, X. Qi, Y. Dong, B. Dai, J. Zhang, Non-Mercury Catalytic Acetylene Hydrochlorination over Bimetallic Au-Ba(Ii)/AC Catalysts. Catal. Sci. Technol. 2015, 5 (3), 1870–1877.
[19] D. Hu, L. Wang, F. Wang, J. Wang, Bimetallic Au-Li/SAC Catalysts for Acetylene Hydrochlorination. Catal. Commun. 2018, 115 (April), 45–48.
[20] K. Zhou, W. Wang, Z. Zhao, G. Luo, J.T. Miller, M.S. Wong, F. Wei, Synergistic Gold-Bismuth Catalysis for Non-Mercury Hydrochlorination of Acetylene to Vinyl Chloride Monomer. ACS Catal. 2014, 4 (9), 3112–3116.
[21] G. Li, W. Li, J. Zhang, Strontium Promoted Activated Carbon-Supported Gold Catalysts for Non-Mercury Catalytic Acetylene Hydrochlorination. Catal. Sci. Technol. 2016, 6 (9), 3230–3237.
[22] J. Regalbuto, Catalyst preparation: science and engineering, CRC Press, 2006.
[23] J.R. Regalbuto, A scientific method to prepare supported metal catalysts, Surface and Nanomolecular Catalysis, (2006) 161-194.
[24] X.Hao, W. Spieker, and J.R. Regalbuto, A Further Simplification of the Revised Physical Adsorption (RPA) Model, Journal of Colloid and Interface Science 267, 2003, 259.
[25] Diao, W., Tengco, J.M.M.T., Gaffney, A.M., Regalbuto, J.R., and Monnier, J.R., Rational Synthesis of Bimetallic Catalysts Using Electroless Deposition Methods, in Catalysis 2020: Volume 32, Spivey, J.J. ed., Roy. Soc. Chem.
[26] M.B. Griffin, A.A. Rodriguez, M.M. Montemore, J.R. Monnier, C.T. Williams, J.W. Medlin, The selective oxidation of ethylene glycol and 1,2-propanediol on Au, Pd, and Au–Pd bimetallic catalysts, Journal of Catalysis, 307 (2013) 111-120.
[27] A.A. Rodriguez, C.T. Williams, J.R. Monnier, Selective liquid-phase oxidation of glycerol over Au–Pd/C bimetallic catalysts prepared by electroless deposition, Applied Catalysis A: General, 475 (2014) 161-168.
[28] J. Rebelli, A.A. Rodriguez, S. Ma, C.T. Williams, J.R. Monnier, Preparation and characterization of silica-supported, group IB–Pd bimetallic catalysts prepared by electroless deposition methods, Catalysis Today, 160 (2011) 170-178.
[29] S.H. Overbury, P.A. Bertrand, and G.A. Somorjai, "The surface composition of binary systems. Prediction of surface phase diagrams of solid solutions," Chem. Rev., 75 (1975) 547.
[30] S. Kristyan and J. Giber, "Temperature dependence of the surface free energies of solid chemical elements," Surf. Sci., 201 (1988) L532.
[31] B.P. Block, J.C. Bailar, The Reaction of Gold(III) with Some Bidentate Coördinating Groups1, Journal of the American Chemical Society, 73 (1951) 4722-4725.

[32] X. Hao, S. Barnes, J.R. Regalbuto, A fundamental study of Pt impregnation of carbon: Adsorption equilibrium and particle synthesis, Journal of Catalysis, 279 (2011) 48-65.
[33] N. Job, S. Lambert, M. Chatenet, C.J. Gommes, F. Maillard, S. Berthon-Fabry, J.R. Regalbuto, J.-P. Pirard, Preparation of highly loaded Pt/carbon xerogel catalysts for Proton Exchange Membrane fuel cells by the Strong Electrostatic Adsorption method, Catalysis Today, 150 (2010) 119-127.
[34] S. Cao, Effect of Nanoparticle Size, Support, and Potassium Dopant on Ruthenium Activity for Levulinic Acid (LA) Hydrogenation to γ-Valerolactone (GVL), (2013).
[35] K. O'Connell, J. Regalbuto, High Sensitivity Silicon Slit Detectors for 1 nm Powder XRD Size Detection Limit, Catalysis Letters, 145 (2015) 777-783.
[36] W. Diao, J.M.M. Tengco, J.R. Regalbuto, J.R. Monnier, Preparation and Characterization of Pt–Ru Bimetallic Catalysts Synthesized by Electroless Deposition Methods, ACS Catalysis, 5 (2015) 5123-5134.
[37] A.G. Sault, R.J. Madix, C.T. Campbell, Adsorption of oxygen and hydrogen on Au(110)-(1 × 2), Surface Science, 169 (1986) 347-356.
[38] Y. Zhang, W. Diao, C.T. Williams, J.R. Monnier, Selective hydrogenation of acetylene in excess ethylene using Ag-and Au–Pd/SiO 2 bimetallic catalysts prepared by electroless deposition, Applied Catalysis A: General, 469 (2014) 419-426.
[39] J. Rebelli, M. Detwiler, S. Ma, C.T. Williams, J.R. Monnier, Synthesis and characterization of Au–Pd/SiO 2 bimetallic catalysts prepared by electroless deposition, Journal of Catalysis, 270 (2010) 224-233.
[40] J. Parmeter, M. Hills, W. Weinberg, Interaction of acetylene with the ruthenium (001) surface, Journal of the American Chemical Society, 108 (1986) 3563-3569.
[41] M. Abon, J. Billy, J.C. Bertolini, Ethylene and acetylene adsorption on a Pt(111) face: Comparative Δφ and coverage measurements, Surface Science, 171 (1986) L387-L394.
[42] K. C. O'Connell, 2016, Characterization, Synthesis And Stabilization Of Au Based Bimetallic Catalysis For The Hydrochlorination Of Acetylene, Doctoral dissertation, Retrieved from https://scholarcommons.sc.edu/etd/3438
[43] P. Johnston, N. Carthey, G.J. Hutchings, Discovery, development, and commercialization of gold catalysts for acetylene hydrochlorination, J. Am. Chem. Soc. 137 (2015) 14548-14557.
[44] B. Dai, Q. Wang, F. Yu, M. Zhu, Effect of Au nano-particle aggregation on the deactivation of the AuCl3/AC catalyst for acetylene hydrochlorination, Scientific reports, 5 (2015).
[45] G. Malta, S.A. Kondrat, S.J. Freakley, C.J. Davies, L. Lu, S. Dawson, A. Thetford, E.K. Gibson, D.J. Morgan, W. Jones, P.P. Wells, P. Johnston, C.R.A. Catlow, C.J. Kiely, G.J., Hutchings, Identification of single-site gold catalysis in acetylene hydrochlorination, Science 355 (2017) 1399-1403.
[46] K. Zhou, J.C. Jia, C.H. Li, H. Xu, J. Zhou, G.H. Luo, F. Wei, A low content Au-based catalyst for hydrodechlorination of C2H2 and its industrial scale-up for future PVC processes, Green Chem. 17 (2015) 356-364.